sustainability

MDPI

Article

Numerical Investigation on the Dynamic Performance of Steel–Concrete Composite Continuous Rigid Bridges Subjected to Moving Vehicles

Binqiang Guo [1], Renzhi Wang [2], Chen Lu [3], Weijian Shi [4] and Qingfei Gao [2,*]

1 Zhejiang Institute of Communications Co., Ltd., Hangzhou 311112, China; guobq@zjic.com
2 School of Transportation Science and Engineering, Harbin Institute of Technology, Harbin 150090, China; 20S032002@stu.hit.edu.cn
3 Zhejiang Hangxuan Expressway Co., Ltd., Hangzhou 310007, China; luchen@zjhxgsglwwgc999.onexmail.com
4 Heilongjiang Provincial Longjian Road and Bridge the First Engineering Co., Ltd., Harbin 150028, China; shiweijian@ljlqygs.com
* Correspondence: gaoqingfei@hit.edu.cn; Tel.: +86-137-0361-6436

Abstract: Assembly construction is the main feature of industrialized bridges, and π-shaped section steel–concrete composites that are continuously rigid have been widely used in engineering fields in recent years; however, their dynamic responses and corresponding impact coefficients in positive and negative moment regions need to be further studied. First, considering the interface slip model, we established a finite element model for the π-shaped continuous region section of the steel–concrete composite on the Sutai Expressway Tongfu No. 3 viaduct. Second, the bridge deck unevenness parameters were generated by preparing a MATLAB program with random calculations and were added to the bridge deck as the excitation load along with the vehicle load. Such parameters are defined on the basis of considering the vertical degrees of freedom of the four wheels and of one vehicle rigid body. Finally, we analyzed the displacement or stress impact coefficients as the dynamic response index of the bridge by adjusting the vehicle travel speeds, vehicle weights, interface slip stiffness values, and deck unevenness values. The results show that the change in vehicle travel speed and the change in vehicle load weight have some influence on the change in the dynamic effect of the combined beam, but this change is not significant. Moreover, the unevenness and interface slip strength changes have a large effect on the dynamic effect of the combination beam, which can significantly change the impact coefficient of the combination beam bridge. The worse the unevenness of the bridge deck is, the lower the grade of interface slip for the steel–concrete composite bridges and the higher the impact coefficient. We calculated the recommended impact coefficient values of the steel–concrete composite bridge based on the specifications for various countries, and they range from 1.16 to 1.4; such values are similar to the finite element calculation results.

Keywords: steel–concrete composite structures; continuous rigid bridges; dynamic performance; moving vehicles; interface slip

check for updates

Citation: Guo, B.; Wang, R.; Lu, C.; Shi, W.; Gao, Q. Numerical Investigation on the Dynamic Performance of Steel–Concrete Composite Continuous Rigid Bridges Subjected to Moving Vehicles. *Sustainability* **2021**, *13*, 13666. https://doi.org/10.3390/su132413666

Academic Editors: Yang Liu, Hongye Gou, Wanshui Han and Jorge de Brito

Received: 13 November 2021
Accepted: 7 December 2021
Published: 10 December 2021

Publisher's Note: MDPI stays neutral with regard to jurisdictional claims in published maps and institutional affiliations.

Copyright: © 2021 by the authors. Licensee MDPI, Basel, Switzerland. This article is an open access article distributed under the terms and conditions of the Creative Commons Attribution (CC BY) license (https://creativecommons.org/licenses/by/4.0/).

1. Introduction

Assembly is the main feature in the industrialization of bridges, and the Chinese Ministry of Transportation has pointed out that the most important methods for improving bridge quality include standardized design, industrialized production, and assembled construction. Compared with reinforced concrete beams, the use of steel–concrete combination beams can shorten the construction period, reduce labor intensity, and lower costs because the mechanical properties of both steel and concrete materials can be fully utilized [1,2].

There are four basic structural systems: simple girder bridges [3], cantilever girder bridges, continuous girder bridges [4], and rigid bridges. Compared with simple girder bridges and cantilever girder bridges, continuous girder bridges involve a reduced number

of expansion joints and an improved linearity and smoothness of the bridge, while rigid bridges involve consolidated main girders and piers, a reduced number of bearings, and a lowered bridge maintenance cost.

Unlike simply supported girders, continuous girders have negative moment [5,6] internal forces in the cross-section near the pivot point under vertical loading. In steel–concrete continuous rigidity, this induces tension in the concrete deck slab, making the concrete slab stress the key control factor for the load performance of the composite girders.

Conventionally assembled steel–concrete composite continuous rigid [7] beams usually consist of independently fabricated steel main girders with concrete deck slabs. Generally, a steel–concrete composite continuous rigid beam is installed first, forming a continuous steel girder before installing the precast concrete deck slab. This construction sequence causes the steel girders and concrete slab to self-weight by the steel girders, and the steel–concrete composite continuous rigid beam bears only the loads that are added later, such as bridge deck pavement and live loads. Second, the steel girders are erected first, and then the bridge deck slab is installed and cannot transport the concrete beam over the steel beam; this means that the beams need to be arranged along the line gantry crane or have access conditions for automobile cranes and other equipment, which limits the application of steel plate combination girders in complex terrain areas. Therefore, the construction sequence of first installing steel girders and then concrete deck slabs will eventually lead to inefficient and inconvenient construction of steel–concrete composite continuous rigid bridge assemblies. In this paper, a π-shaped combination beam, which is prefabricated in a factory and lifted on site, has a high combination efficiency and strength to meet the construction (beam-on-beam transportation) strength requirements, sufficient construction performance, and is suitable for construction in mountainous areas and other complex terrains.

As a new type of cementitious material, ultra-high-performance concrete [8] (UHPC) has the advantages of high strength and excellent durability. A team of Massachusetts Institute of Technology (MIT) [9] and Cambridge University researchers first explored the structural optimization of prestressed UHPC that was simply supported girders and found that π-sections with foot heels are best suited for the requirements of typical high-speed bridges while significantly reducing the overall construction cycle time and providing a high load carrying capacity, high durability, and appropriate prestressing effect. In 2001, the Federal Highway Administration [10] (FHWA) began to develop a modular, standard-size prestressed UHPC precast π-beam with a 23–41 m factory prefabrication span and rapid on-site assembly and installation. Additionally, the transverse connection of this series of precast girders was in the form of cast-in-place UHPC transverse joints. A test bridge was built in Virginia in 2004 in the U.S., showing the advantages of this type of bridge with fast construction speed. Starting in 2012, FHWA [11] developed the second generation of UHPC precast π-girders, which was more practical with respect to optimized construction compared to the first generation (2001).

China follows the international research frontier, and with the research on the structure system, developing fewer main beam systems has become the new development direction. The Huaihe River Bridge on the Jiqi Expressway in Anhui Province [12] was the first bridge in which the double I-beam plate combination girder bridge form was adopted. Shi Xuefei [13] studied a double I-beam combination beam bridge from the perspective of reducing the amount of steel used for a more comprehensive analysis of the structural parameters. The Hunan Changyi Expressway expansion project [14] was the first in which the steel plate combination girder structure was adopted; this was a useful attempt to adopt the assembled steel plate combination girder structure under complex terrain conditions in a hilly mountainous area in China. Su Qingtian proposed a π-shaped steel plate girder formed by connecting two I-beams with crossbeams instead of with a single I-beam, and the single group of beams was lifted onto the support as a whole after the construction was completed.

Due to the influence of the expansion joints, the travel comfort of simply supported girder bridges is worse than that of continuous girder bridges, and steel–concrete composite continuous rigid beam bridges should be given special attention. The corresponding negative moment zone [15,16] represents the state of concrete under tension and steel main girders under pressure; this is extremely unfavorable to the normal use of bridges and even affects the safety performance of bridges. Therefore, dynamic performance research on steel–concrete composite continuous rigid bridges is especially important.

In this paper, a π-section steel–concrete composite continuous rigid bridge FEM was built, and its dynamic performance was studied. In this model, the different parameters, including vehicle travel speeds, vehicle weights, interface slip stiffness values, deck unevenness values, and different positions of sections, from the left first point of support to the right first point of support, are carefully considered.

2. Finite Element Model

The Sutai Expressway is one of the six major corridors from Zhejiang to Jiangsu, connecting two of China's most economically developed provinces. Tongfu Elevated Bridge No. 3 is located at K25 to K27 of the Sutai Expressway, where the 3rd to 5th, 7th to 8th, and 10th to 14th couplings are π-section continuous rigid steel–concrete composite continuous rigid beams.

In this paper, the third 5 × 30 m continuous girder with a transverse bridge width of 2 × 16.5 m is selected for analysis, and each girder is composed of four π-bay combination girders. Each girder consists of two I-beam Q355 steel girders that are 1.18 m in height, 0.3 m in flange length, and 0.024 m in plate thickness, and have one C50 concrete deck plate that is 0.4 m in thickness. The cross-sectional schematic is shown in Figure 1.

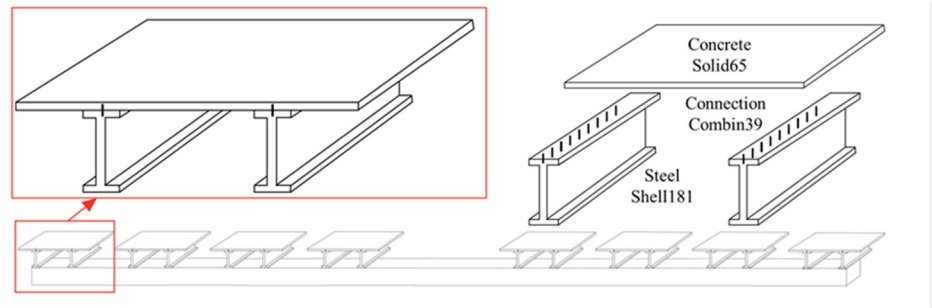

Figure 1. Cross-sectional pictures of the beam.

Each girder has a web thickness of 16 mm. Its wing width is 300 mm, and its web thickness is 16 mm. The spacing between the two girders is 2.1 m; the girders are fastened to the abutment cover beam with welded nails and anchor bars. Each support point is made of an H-shaped reinforced concrete abutment, and the foundation is made of reinforced concrete bored piles.

ANSYS solid 65 [17–19] was used as the simulation unit of the concrete bridge deck, and shell181 [20] was used as the simulation unit of the steel main girder to construct the shell body unit model of the steel–concrete composite continuous rigid beam with a π-shaped section, as shown in Figure 2. Subsequently, the vibration simulation model of steel–concrete composite continuous rigid bridges is established and discussed for the positive moment region and negative moment region of the continuous combined girder bridge.

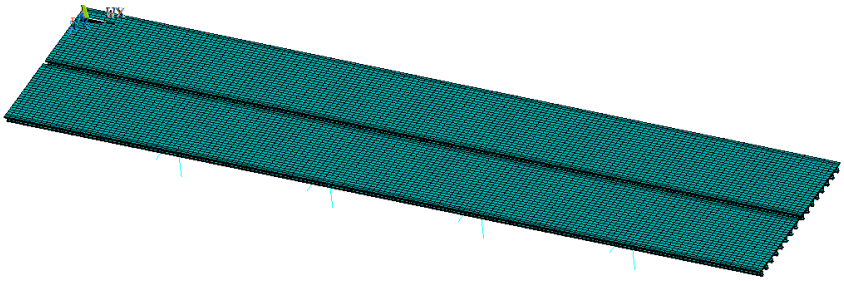

Figure 2. π-section steel–concrete composite continuous rigid bridge model.

The interface slip effect of steel–concrete composite girder bridges has an influence [21] on the dynamic performance of the combined girder bridges. With the generation of interface slip, the overall stiffness of the combined girder decreases, the self-oscillation frequency decreases, and the dynamic performance subsequently increases. Therefore, it is necessary to consider the effect of the interface slip change on the dynamic performance of steel–concrete composite continuous rigid bridges.

In the Tongfu No. 3 viaduct, the interface connection of the concrete deck plate and the steel main beam is achieved with shear nails, which are used as pinned connections to connect the concrete deck plate to the steel main beam. As one of the flexible connectors, the load–slip displacement principal structure relationship of the shear pegs can be described by exponential functions [22,23], such as $(1 - e^{-m \cdot x})^n$, or hyperbolic functions [24], such as $\frac{a \cdot x}{1+b \cdot x}$. Among others, Ollgaard and Buttry [25] defined more classical load–slip displacement equations, as shown in Equations (1) and (2).

$$Q = Q_u \left(1 - e^{-18x}\right)^{\frac{2}{5}} \tag{1}$$

$$Q = Q_u \frac{80x}{1 + 80x} \tag{2}$$

In the above equations, x is the interface slip displacement (in), Q is the peg shear force (kN), and Q_u is the bearing capacity design value (kN) of the shearing nails [26,27]. According to the above load–slip curve, when the slip displacement length is 0.2 in, i.e., 5.08 mm or more, the peg shear force Q accounts for more than 94% of the design value of the peg's shear bearing capacity Q_u; this can be considered peg failure. In addition, when the slip displacement is 0.0125 in, i.e., 0.3175 mm, the peg shear force Q is already approximately 50% of the design value of the peg's shear load capacity Q_u. Therefore, describing the load–slip displacement performance is feasible for the shear pegs of the Tongfu No. 3 viaduct by using the fold line from the second to the third section.

From Equations (1) and (2), it is clear that to obtain a true and reliable relationship between shear studs and slip displacement, the design value of the stud shear bearing capacity must be calculated accurately. In this paper, we also use Ollgaard's formula for the stud connector shear strength (Q_u) [28], according to the actual condition of the Tongfu No. 3 viaduct. As shown in Equation (3), the design value of the shear bearing capacity of its individual pegs can be calculated.

$$Q_u = 0.43 A_s \sqrt{f_c E_c} = 0.43 \times (\pi \times 121) \times \sqrt{23.1 \times 34.5 \times 10^3} = 145\text{kN} \tag{3}$$

In the finite element model (FEM) of the Tongfu No. 3 viaduct, the concrete solid unit and the steel main girder slab unit can be connected by a COMBIN No. 39 [29] nonlinear spring unit to simulate the interface slip of the combined girder bridge. COMBIN No. 39 is a unidirectional element with nonlinear generalized force deflection capability, which also has a longitudinal capability in 3D applications. This spring unit creates a three-way spring between the concrete deck plate and the steel main beam, and the load–displacement curve in each direction can be described by a generalized force–deformation curve, as shown

in Figure 3. Therefore, the transverse and vertical bridge direction degrees of freedom at the corresponding nodes of the concrete slab and the steel main beam are coupled in the COMBIN No. 39 nonlinear spring cell of the combined girder FEM of the Tongfu No. 3 viaduct. Subsequently, in reference to Oehlers' [29] analysis of 116 pinned concrete slab test data with Zhang Shipo [30] with the improved calculation method for the shear stiffness of the combined beam peg shear connectors, the force–deformation curve was defined with 0.5 Q_u as the dividing point; the load–slip relationship in the longitudinal bridge direction of the pegs in this model was represented by two straight lines, as shown in Figure 3 and Table 1. This change in the load set also induces a change in the self-oscillation frequency of the bridge, as shown in Table 1.

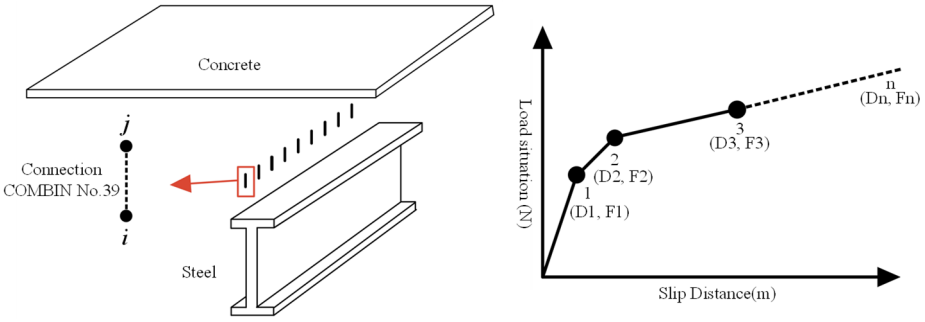

(**a**) COMBIN No. 39 application

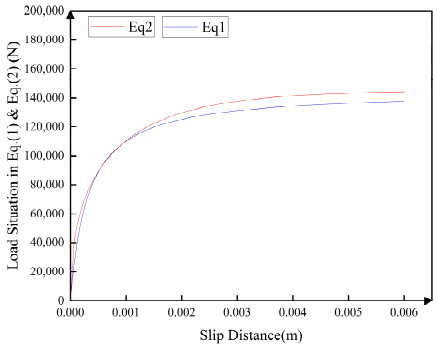

(**b**) Equations (1) and (2)

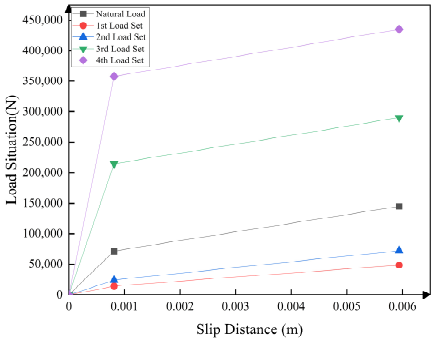

(**c**) Work conditions load–slip

Figure 3. Load–slip behavior.

Table 1. Frequencies of different steel–concrete composite bridge interface load–slip behaviors.

Name	K_1	K_2	f_1	f_2
Natural Load	8.79×10^6	1.43×10^7	2.99	3.21
1st Load Set	1.76×10^7	6.64×10^6	2.58	2.79
2nd Load Set	2.93×10^7	9.49×10^6	2.70	2.90
3rd Load Set	2.64×10^8	1.47×10^7	3.21	3.47
4th Load Set	4.40×10^8	1.51×10^7	3.27	3.51

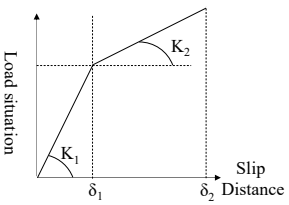

Bridge deck unevenness is the main influencing factor of bridge dynamic performance [31,32], and the most vital aspect for vehicle travelling excitation is the unevenness of the bridge deck, which must be considered in the vehicle–bridge coupling analysis. We adopted roadway power spectrum theory to simulate bridge deck unevenness, treating the unevenness of the bridge deck as a smooth random process for the ephemeral, zero mean, and Gaussian probability distribution of each state [33,34]. In this paper, the unevenness parameters are calculated randomly with a prepared MATLAB program and are

obtained as a set of series and added to the bridge deck as the excitation load along with the vehicle load.

In Table 2, different levels of bridge deck unevenness parameters are generated by controlling the power spectrum density of the bridge deck unevenness coefficients to obtain five types of bridge deck unevenness samples. Typical power spectrum density function [35] can be approximated by an exponential function, as shown in Equation (4):

$$S(\gamma) = \alpha\gamma^{-\beta}; \quad \gamma_a < \gamma < \gamma_b \tag{4}$$

α: Roughness coefficient.
β: Spectral shape index.
γ: Spatial frequency, with γ_a and γ_b as the lower and upper limits.

Table 2. The unevenness coefficient value of the bridge deck.

Grade of the Bridge Deck	α (m^3/Circle)	α (m^3/Circle)
Excellent	$\alpha \leq 0.24 \times 10^{-6}$	0.1×10^{-6}
Good	$0.24 \times 10^{-6} < \alpha \leq 1 \times 10^{-6}$	0.5×10^{-6}
Normal	$1 \times 10^{-6} < \alpha \leq 4 \times 10^{-6}$	2×10^{-6}
Bad	$4 \times 10^{-6} < \alpha \leq 16 \times 10^{-6}$	2×10^{-6}
Terrible	$16 \times 10^{-6} < \alpha$	20×10^{-6}

The bridge deck unevenness was simulated by using a fast Fourier inverse transform to generate uneven samples. MATLAB R2019b software was used to establish the axle vibration simulation model of steel–concrete composite continuous rigid bridges considering the unevenness of the roadway.

The impact coefficient is influenced by the bridge fundamental frequency [36]. The FEM of steel–concrete composite continuous rigid bridges with π-shaped cross-sections established in this paper can accurately simulate the vibration pattern and frequency of the bridge, as shown in the first-order and second-order combination beam vertical formations in Figure 4. Then, reasonable bridge samples and reasonable vehicle samples are selected to simulate the bridge deck unevenness by using fast Fourier inversion, and uneven samples are generated using MATLAB R2019b software to establish the bridge vibration simulation model of steel–concrete composite continuous rigid bridges considering the unevenness of the roadway. The displacement impact coefficient and strain impact coefficient are used as the dynamic performance indexes, and the analysis is carried out on both the positive moment region and negative moment region of the continuous beam. Varying the bridge deck unevenness, vehicle travel speed, vehicle weight, and steel–concrete joint strength, the effects of the variations in these factors on the impact coefficients at different locations are explored.

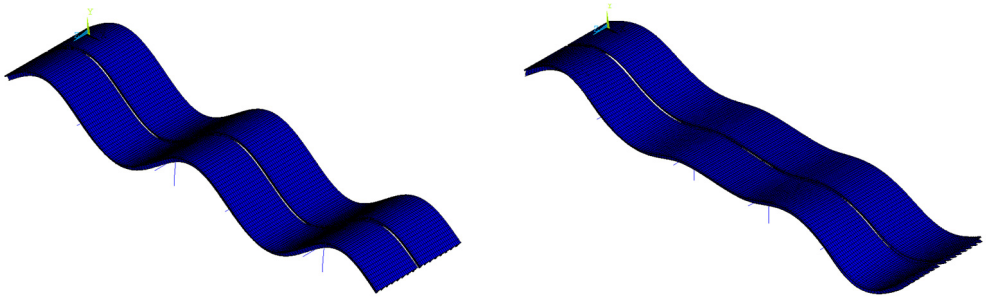

(**a**) First-order frequency (**b**) Second-order frequency

Figure 4. Frequency of π-section steel–concrete composite continuous rigid bridges.

There are many types of mobile vehicles [37,38]. For this study, we chose a four-wheeled vehicle model. Considering the vertical degrees of freedom of the four wheels

and the vertical degrees of freedom of the vehicle rigid body, the distance between the front and rear axles of the vehicle is 3 m, the front and rear axle distance is 2 m, and the wheelbase-to-wheelbase ratio is 0.67; these parameters reflect the real running vehicle situation and can be accurately coupled with the bridge model. The vehicle model was established with this information, meaning that different vehicle parameters (including spring stiffness and mass) will change the vehicle frequency. Five different weights of vehicles, including 20 t, 25 t, 30 t, 35 t, and 40 t, are considered, and their frequencies are shown in Table 3. The FEM of the loaded vehicle is shown in Figure 5.

Table 3. Vehicle weight and frequency values.

Number	Weight of Vehicle	Frequency of Vehicle
W-20	20 t	1.233
W-25	25 t	1.102
W-30	30 t	1.006
W-35	35 t	0.932
W-40	40 t	0.872

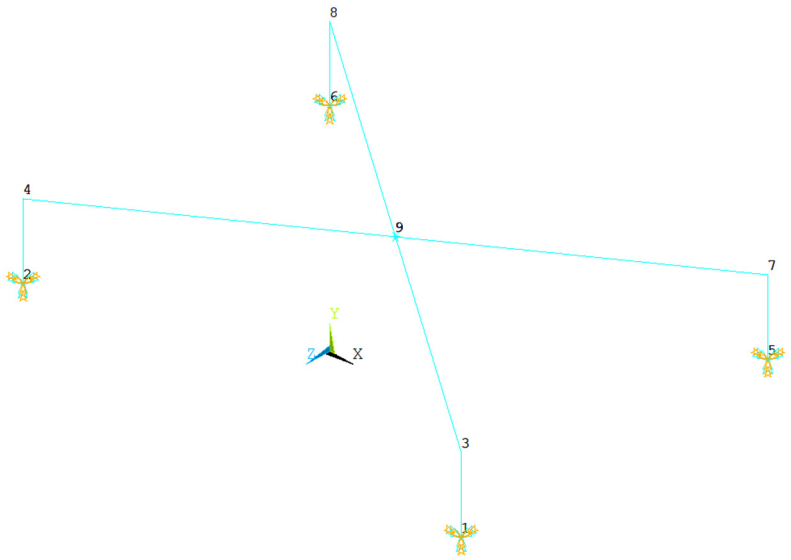

Figure 5. The FEM of the loaded vehicle.

The FEM, the loading model, and the load–slip behavior of steel–concrete composite continuous rigid bridges were verified according to previous field work. Qingfei and Gao developed [37] the VBCVA program for this kind of coupled vibration analysis of vehicle bridges and verified its correctness. Moreover, other structures, such as T-shaped steel–concrete composite simple-supported beam bridges, could also use this model. In this paper, the bridge impact coefficients are selected as the dynamic performance index. The dynamic performance when the vehicle crosses the bridge is greater than the static deflection when the vehicle is stationary, so the impact coefficient concept is introduced through national codes to reflect the dynamic performance effect of the bridge under the action of a moving vehicle load. This paper adopts the Chinese code D60-2004 [36] provisions of the impact coefficient, as shown in Equation (5).

$$\eta = \frac{\delta_{d\max}}{\delta_{j\max}} \tag{5}$$

$\delta_{j\max}$: The maximum static effect of the vehicle load under the action of the load value.
$\delta_{d\max}$: For the bridge in the effect of the time curve, the maximum static effect at the maximum dynamic performance value.

3. Dynamic Performance of the Positive Moment Zones

Unlike the simply supported girders, the multispan continuous girders need to bear the negative bending moment at each mid-span in addition to the positive bending moment at each mid-span under the vertical moving load, such as that induced by vehicles. Therefore, the bridge span can be divided into two parts [38]: the positive moment zone, including five areas in the side span, second side span and middle span; and the negative moment zone, including the left support point, left middle support point, right middle support point, and right support point. In Figure 6, the red area is the negative moment zone, the blue area is the positive moment zone, and the vehicle is driven from left to right. This paper first studies the dynamic performance of the bridge structure in the positive moment zone, including the middle of the side span, the middle of the second side span, and the middle of the middle span at different section positions. Second, the dynamic performance of the bridge is studied in the negative moment zone at different cross-sectional locations, including the top of the side pier and the top of the middle pier.

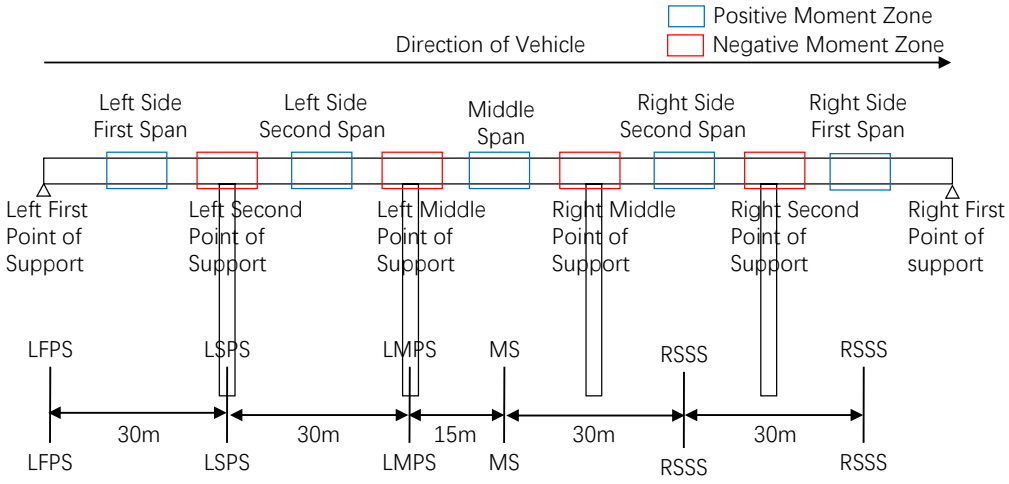

Figure 6. Position of the moment zones and sections.

Since the concrete is constructed with the Solid65 solid unit and the steel girders are constructed with the Shell181 plate unit, the vertical displacements in the positive moment region and the concrete strains in the parallelogram direction with the concrete strains in the negative moment region are extracted. Additionally, the dynamic performance effect of the bridge under the action of the moving vehicle load is calculated by applying Equation (5). The specific parameters extracted for different locations and their section abbreviations are shown in Table 4.

Table 4. Section names and moment zones.

X Position	Abbreviation	Section Name	Moment Zone	Post-Process Value
0	LFPS	Left First Point of Support	-	-
15	LSFS	Left Side First Span	Positive	Y Displacement
30	LSPS	Left Second Point of Support	Negative	X Stress
45	LSSS	Left Side Second Span	Positive	Y Displacement
60	LMPS	Left Middle Point of Support	Negative	X Stress
75	MS	Middle Span	Positive	Y Displacement
90	RMPS	Right Middle Point of Support	Negative	X Stress
105	RSSS	Right Side Second Span	Positive	Y Displacement
120	RSPS	Right Second Point of Support	Negative	X Stress
135	RSFS	Right Side First Span	Positive	Y Displacement
150	RFPS	Right First Point of Support	-	-

In our investigation, a 30 t vehicle was driven across the whole bridge at a constant speed. The bridge deck evenness level was very good, the speed was taken every 20 km/h, from 40 to 80 km/h was additionally tested.

To consider the changes in the vehicle driving speed, six finite unit models were established to extract the maximum dynamic stress value of the steel main beam in the positive moment zone and calculate the corresponding maximum static stress value. The positive calculated values of the vertical bridge impact coefficients in the moment zone are shown in Figure 7.

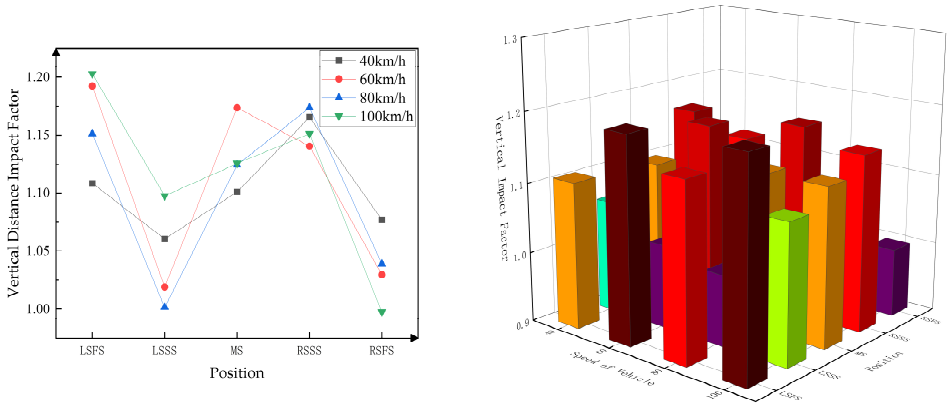

(**a**) Impact coefficients 2D line chart (**b**) Impact coefficients 3D histogram

Figure 7. Vertical impact coefficient values of steel–concrete composite continuous rigid bridges based on the vehicle travel speed.

Figure 7 shows that the value of the vertical displacement impact coefficient of steel–concrete composite continuous rigid bridges is evidently influenced by the vehicle travel speed, and the change in vehicle travel speed causes a large change in the vertical impact coefficient of the middle span section in the positive moment region at different positions. The vertical displacement impact coefficients of the combined girders show a fluctuating trend with the change in vehicle speed, in which the vertical displacement vertical impact coefficients of the left side second span (LSSS) are relatively sensitive to the influence of vehicle speed, while these coefficients of the right side second side span and middle span change less. In the early stage of bridge structure deterioration, the second span of the bridge is more affected by the dynamic performance, and the second span structure needs to be checked more frequently.

Therefore, as other factors are explored, the longitudinal impact coefficients in different spans, in the cross-sectional distribution of the more obvious impact coefficient value for the 80 km/h vehicle speed, lead to impact coefficient changes in the general vehicle speed, unevenness, vehicle weight, and connection strength, and other influencing factors for further analysis.

As the traffic volume increases, the mainline combination bridge carries heavier and heavier vehicles, and the change in the vehicle weight changes the vehicle frequency; this in turn affects the impact coefficient of the steel–concrete composite continuous rigid bridges to a great extent. Therefore, as the driving vehicle with a vehicle weight and frequency taken as shown in Table 3 is driven across the full bridge at a constant speed of 80 km/h, the unevenness of the bridge deck is set to be better than before. According to the vehicle weight and working conditions shown in Table 3, five finite unit models are established. The vertical displacements of the left/right side span, left/right second side span, and the middle spansections of the steel–concrete composite continuous rigid bridges are numerically simulated and extracted, and their impact coefficients are calculated, as shown in Figure 8.

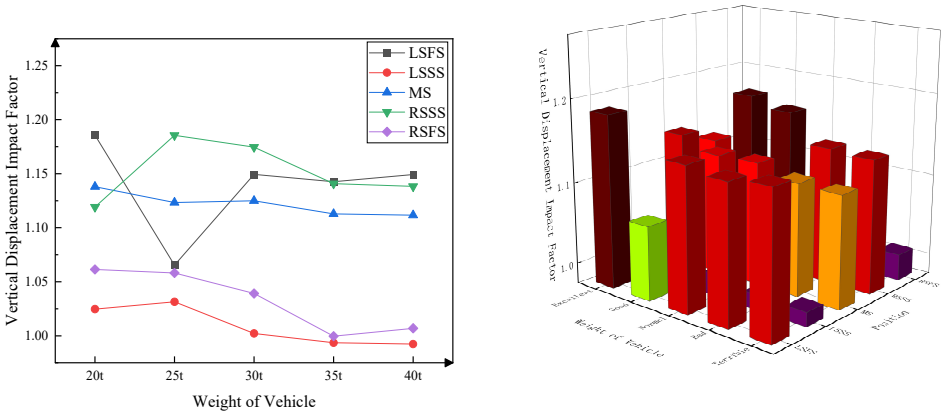

(**a**) Impact coefficient 2D line chart (**b**) Impact coefficient 3D histogram

Figure 8. Values of the distance impact coefficient with changing vehicle weight.

Figure 8 shows that the values of the vertical displacement impact coefficient of the steel–concrete composite continuous rigid bridges do not change significantly with the change in vehicle weight. Except for the vehicle weight of 25 t and the position of the left side first span (LSFS), where the vertical displacement impact coefficient exhibits a sudden change, the displacement impact coefficients of the cross-sections and vehicle weights do not change significantly. The reason for this is that after the vehicle weight changes, the vehicle frequency changes from 0.872 to 1.223 Hz, while the bridge frequency is 2.5 Hz to 3.5 Hz. Additionally, the change value of the vehicle frequency is not significant compared with the bridge frequency, meaning that the vehicle weight change does not significantly affect the displacement impact coefficient of the steel–concrete composite continuous rigid bridge.

The change in vehicle travel speed and the change in vehicle weight represent the changes in structural dynamic performance caused by the change in load. However, along with the ageing of the combined girder bridge, the concrete pavement unevenness increases, and structural defects of the steel–concrete composite continuous rigid bridges gradually appear, leading to changes in the deck unevenness or changes in the steel–concrete composite rigid interface slip relationship. Such changes differ from other factors in that they act directly on the combined girder bridge itself, reducing the load carrying capacity of the combined girder bridge semi-permanently until repair, posing a certain threat to the bridge structure operation and maintenance, and thus requiring a focused analysis.

The change in bridge deck unevenness has a large impact on the impact coefficient of the steel–concrete combination girder bridge. Therefore, 30 t vehicles were driven across the whole bridge at a constant speed of 80 km/h, with the bridge deck unevenness shown in Table 2. Then, the change in vehicle speed is considered, and five finite unit models are established. The cross-bridge displacement and vertical displacement of the side span, middle span, and second side span section of the steel–concrete composite rigid bridge are extracted, and the impact coefficient is calculated, as shown in Figure 9.

Figure 9 shows that the values of the vertical displacement impact coefficients of the steel–concrete composite rigid bridge all increase significantly as the bridge deck unevenness changes from very good to good, fair, poor, and very poor. However, the magnitudes of change in the vertical displacement impact coefficients of the steel–concrete composite rigid bridge with different cross-sections are different, and the sensitivity to unevenness of the bridge deck is not the same. It can be clearly observed from the three-dimensional diagram that the section that is most sensitive to the unevenness of the bridge deck is the right side second span (RSSS), and in contrast, the section that is least sensitive to the unevenness of the bridge deck is the left side first span (LSFS). Therefore, in the inspection of structurally similar steel–concrete composite rigid bridges, the second side

spans (RSSS and LSSS) require more frequent inspection than the first side spans (RSFS and LSFS).

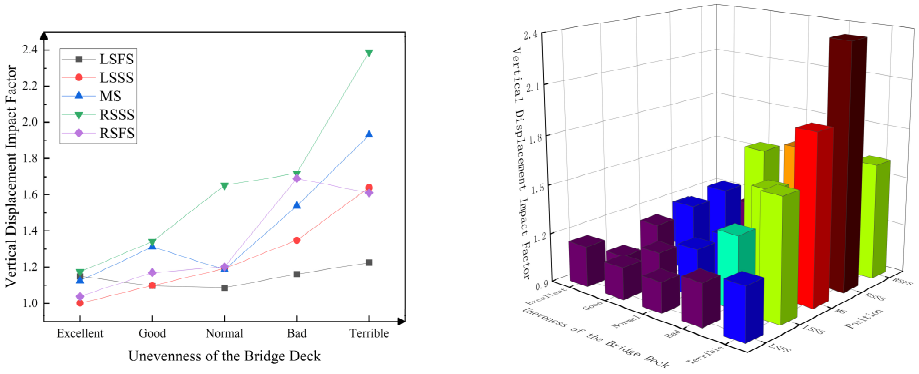

(**a**) Impact coefficient 2D line chart (**b**) Impact coefficient 3D histogram

Figure 9. Values of the distance impact coefficient with changing bridge deck roughness.

In the service process, the connection strength of the steel–concrete composite rigid bridge is reduced by the pins, and the structural defects of the steel–concrete composite rigid bridge gradually appear, resulting in a change in the interface load–slip behavior of the steel–concrete composite bridge. This change in the slip relationship induces a change in the self-oscillation frequency of the bridge, and as shown in Table 4, the higher the connection strength is, the smaller the vertical first-order and second-order self-oscillation frequency values of the bridge.

Figure 10 shows that the rise in the connection grade of the combination girders has an obvious effect on the vertical displacement impact coefficient of this combination girder bridge, and the degree of change in the vertical displacement impact coefficient is different at different locations. In particular, the value of the vertical displacement impact coefficient of the combination girder at the RSSS section position is higher than that at the other positions. In general, as the connection condition between the concrete deck plate and the steel main beam increases, the overall stiffness of the bridge increases and the interface slip connection stiffness decreases, resulting in a lower bridge frequency that is closer to the vehicle frequency, and the corresponding impact coefficient becomes larger. The effects of different parameters and different positions on the impact coefficients are shown in Table 5.

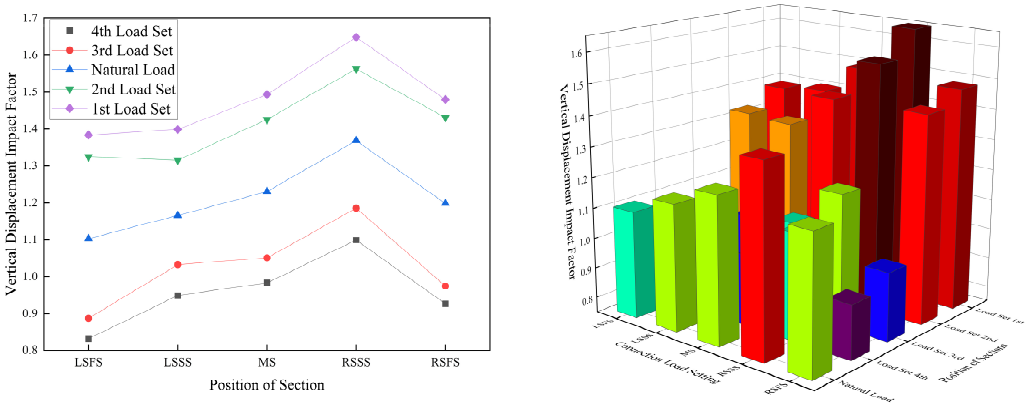

(**a**) Impact coefficient 2D line chart (**b**) Impact coefficient 3D histogram

Figure 10. Values of the vertical distance impact coefficients with different interface load–slip behaviors.

Table 5. The effect of the parameters and positions of impact coefficients in positive moment zones.

Section Position	LSFS(RSFS)	LSSS(RSSS)	MS
Vehicle travel speed	Not significant	Not significant	Higher but not significant
Weight of vehicle	Not significant	Not significant	Not significant
Bridge deck roughness	Positive correlation	Positive correlation	Higher and positive correlation
Interface slip behavior	Lower and negative correlation	Negative correlation	Negative correlation

4. Dynamic Performance of the Negative Moment Zones

For a steel–concrete composite continuous rigid bridge with a span diameter of 5×30 m, considering the vertical load of the driving car, the side pivot section and the middle pivot section [39] were loaded with a negative bending moment while the car was driving across the bridge, and this loading situation led to tension at the upper edge and compression at the lower edge of the combination girder section. In π-shaped girders, the concrete deck slab was located on two I-beams. When loaded with a negative bending moment, the concrete deck slab is under tension, and the steel main beam is under pressure, resulting in concrete cracking and other deck damage in the negative moment region. Because this damage comes from the vehicle load, it is necessary to investigate the dynamic performance of vehicle driving in the negative moment zone at the side and middle support points of the continuous beam.

To investigate the influence of the bridge deck unevenness on the impact coefficient in the negative moment zone of the steel–concrete composite continuous rigid bridge, five finite element models were constructed. These models range from very poor to very good unevenness, and a 30 t vehicle was driven across the whole bridge in a straight line at a constant speed of 80 km/h. The maximum strain values at the secondary edge support point and the middle support point of the steel–concrete composite continuous rigid bridge was extracted, and the impact coefficients corresponding to different locations and different bridge deck unevenness were calculated.

Figure 11 shows that the longitudinal strain impact coefficient in the negative moment zones of the steel–concrete composite continuous rigid bridge increases sharply with the deterioration of the bridge deck unevenness from very good to very poor at different pivot positions of the continuous girder; this variation is large, from approximately 1.1 to a maximum of 1.8. The reason for this is that the unevenness of the bridge deck mainly changes the main load excitation of the bridge when the vehicle is driving on the bridge; the unevenness also has an impact on the bridge. The impact coefficient is smaller when the unevenness is very good and larger when the unevenness is very poor.

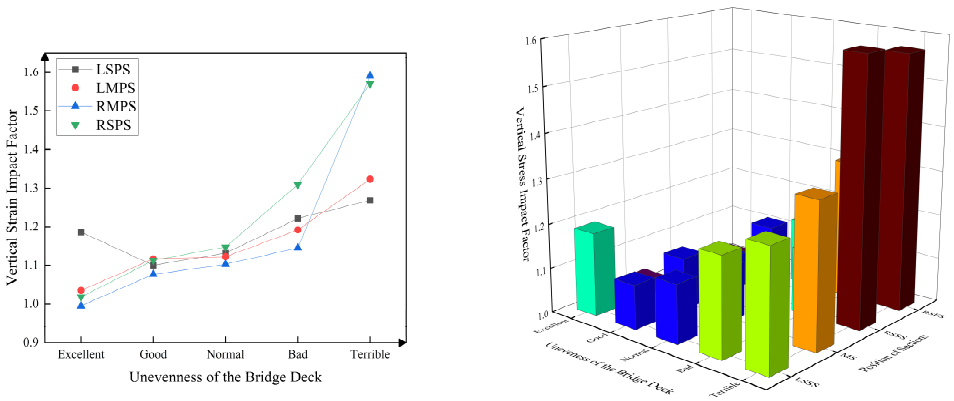

(**a**) Impact coefficient 2D line chart (**b**) Impact coefficient 3D histogram

Figure 11. Values of the strain impact coefficient with changing bridge deck roughness.

The vehicle weight variation changes the vehicle frequency, which in turn affects the impact coefficient of steel–concrete composite continuous rigid bridges. Therefore, in the excellent bridge case, the five separate vehicles shown in Table 2 were constructed to drive across the full bridge in a straight line at a uniform speed of 80 km/h. Then, the transverse strain and vertical strain of each negative moment zone pivot section of the steel–concrete composite continuous rigid bridge were extracted, and the impact coefficients were calculated, as shown in Figure 12.

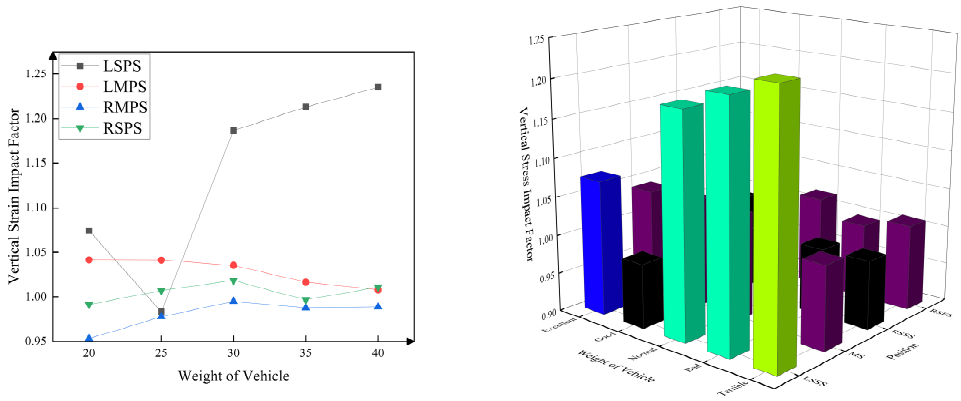

(**a**) Impact coefficient 2D line chart (**b**) Impact coefficient 3D histogram

Figure 12. Values of the strain impact coefficient with changing vehicle weight.

Figure 12a shows that the longitudinal strain impact coefficient in the negative moment region of the steel–concrete composite continuous rigid bridge does not change much with the change in vehicle weight and is concentrated at approximately 1.0, except for LSPS. The figure also shows that the transverse strain impact coefficient is concentrated at approximately 1.1, remaining almost constant with increasing vehicle weight. This indicates that the increase in vehicle weight has a small effect on the dynamic performance of vehicle driving in the negative moment zone at the side and middle pivot points of the continuous beam. The effects of different parameters and different positions on the impact coefficients are shown in Table 6.

Table 6. The effect of the parameters and positions of impact coefficients in negative moment zones.

Section Position	LSFS(RSFS)	LSSS(RSSS)
Weight of vehicle	Not significant	Not significant
Bridge deck roughness	Higher and positive correlation	Positive correlation

5. Discussions

In this study, we collected the relevant automobile load impact coefficient provisions in the codes implemented in various countries to calculate the impact coefficients of the π-section steel–concrete composite continuous rigid bridge in link 3 of the Sutai Expressway. The calculation methods specified in these codes can be divided into four categories [16] according to the independent variables and the live load model, including the bridge span and bridge fundamental frequency as independent variables, which are related to the limit condition and considered in the live load model.

The first type of calculation method uses the bridge span as the independent variable to calculate the bridge impact coefficient. Countries that use this method include the former Soviet Union, India, Japan, Italy, Germany, New Zealand, Korea, and Latvia [40]; the corresponding formula is shown in Equation (6), where the only variable L is the bridge span. The second type of calculation method uses the base frequency of the bridge to calculate the impact coefficient of the bridge. Countries that use this type of calculation method include China and Switzerland; the corresponding formula is shown in Equation (7), where the

only variable f is the base frequency of the bridge. The third type of impact coefficient calculation method considers the impact coefficients in different limit states. The main code that relies on this method is the American AASHTO LRFD code, which distinguishes between the impact coefficients of all bridge deck slab limit states and the fatigue fracture limit states of other members and other limit states. The fourth type of impact coefficient is calculated by incorporating the impact technique into the live load model. Countries using this approach include the United Kingdom, Finland, Spain, Norway, Sweden, South Africa, and other countries that utilize dynamic performance. The canonical impact coefficients taken in the live load static model are included in this model. Typical impact coefficients for the third and fourth categories are shown in Equation (8).

$$\begin{array}{l} impact\ factor\ of\ USSR = \frac{15}{37.5+L} + 1 \\ impact\ factor\ of\ India = \frac{9}{13.5+L} + 1 \\ impact\ factor\ of\ Japan = \frac{20}{50+L} + 1 \\ impact\ factor\ of\ Italy = \frac{(100-L)^2}{100\times(250-L)} + 1 \\ impact\ factor\ of\ Germany = 0.4 - 0.008L + 1 \\ impact\ factor\ of\ NZL = \frac{15}{38+L} + 1 \\ impact\ factor\ of\ Korea = \frac{15}{40+L} + 1 \\ impact\ factor\ of\ LATVIA = \frac{15}{37.5+L} + 1 \end{array} \quad (6)$$

L: Span length of the bridge.

$$\begin{array}{l} impact\ factor\ of\ China = 0.1767 \ln f - 0.0157 + 1 \\ impact\ factor\ of\ Switzerland = 0.4 + 1 (when\ 2 < f < 4) \end{array} \quad (7)$$

f: Fundamental frequency of the bridge.

$$\begin{array}{l} impact\ factor\ of\ ENG = 0.25 + 1 \\ impact\ factor\ of\ Finland = 0.4 + 1 \\ impact\ factor\ of\ USA = 0.33 + 1 \end{array} \quad (8)$$

In accordance with the specification impact coefficient formula, the impact coefficient of the third link bridge of the Tongfu No. 3 viaduct is calculated, as shown in Table 7. The impact coefficients range from 1.16 to 1.4 for each country; this range is compatible with the range of impact coefficients calculated in this paper. In the above analysis, the impact coefficients at different locations on a bridge have different variation patterns, and these impact coefficients should be taken as the maximum impact coefficient of the bridge according to the most unfavorable principle.

Table 7. Impact coefficient values in different countries.

China	U.S.S.R.	India	Japan	Germany	N.Z.L.
1.2222	1.2222	1.2069	1.2500	1.1600	1.2206
Korea	Latvia	Switzerland	Finland	U.K.	U.S.
1.2143	1.2222	1.4000	1.400	1.2500	1.3300

6. Conclusions

(1) The change in vehicle speed and vehicle load weight have some influence on the change in the dynamic performance of the combined beam; however, the change is not significant, and the displacement and strain impact coefficients are between 1.0 and 1.2 at different cross-sectional positions.

(2) Unevenness and steel–concrete connection strength changes have a large impact on the dynamic performance of the combined beam, which can significantly change the impact coefficient of the combined beam bridge. The worse the unevenness of the bridge

deck, the lower the connection stiffness of the combined girder, and the higher the impact coefficient of the combined girder, ranging from 1.0 to 2.2.

(3) In the positive moment zone, the displacement impact coefficient is higher at the right side second span (RSSS) and middle span (MS); in the negative moment zone, the strain impact coefficient is higher at the left side point of the support (LSPS) position. However, the change is not significant, being less than 20%.

(4) The maximum impact coefficients of steel–concrete composite continuous rigid bridges can be calculated in each country according to their numerical sources, which are classified into four types: span diameter, base frequency, limit condition and load model. According to the impact coefficient calculation formulae of different countries, in this paper, we calculated the recommended values of impact coefficients from 1.16 to 1.4, which are similar to the finite element calculation results.

Author Contributions: Conceptualization, B.G., W.S. and Q.G.; methodology, B.G. and Q.G.; software, R.W. and C.L.; validation, B.G., R.W., and W.S.; formal analysis, R.W. and C.L.; investigation, B.G. and W.S.; resources, C.L. and Q.G.; data curation, R.W. and Q.G.; writing—original draft preparation, B.G. and R.W.; writing—review and editing, W.S. and Q.G.; supervision, C.L. and Q.G.; project administration, C.L. and W.S.; and funding acquisition, Q.G. All authors have read and agreed to the published version of the manuscript.

Funding: This study was funded by the Key Research & Development Program of Shandong Province of China (grant no. 2019JZZY010427).

Data Availability Statement: Not applicable.

Conflicts of Interest: The authors declare that they have no known competing financial interests or personal relationships that could appear to influence the work reported in this paper.

References

1. Nie, J.; Wang, J.; Gou, S.; Zhu, Y.; Fan, J. Technological development and engineering applications of novel steel-concrete composite structures. *Front. Struct. Civ. Eng.* **2018**, *13*, 1–14. [CrossRef]
2. Nie, J.; Tao, M.; Wu, L.; Nie, X.; Lei, F. Advances of research on steel-concrete composite bridges. *China Civ. Eng. J.* **2012**, *45*, 110–122. [CrossRef]
3. González, A.; Mohammed, O. Dynamic Amplification Factor of Continuous versus Simply Supported Bridges Due to the Action of a Moving Vehicle. *Infrastructures* **2018**, *3*, 12. [CrossRef]
4. Deng, L.; He, W.; Shao, Y. Dynamic Impact Factors for Shear and Bending Moment of Simply Supported and Continuous Concrete Girder Bridges. *J. Bridge Eng.* **2015**, *20*, 04015005. [CrossRef]
5. Tangwongchai, S.; Lertsima, C.; Chucheepsakul, S. Suitable effective strip width of continuous bridge deck slabs system over flexible steel I-girders. *J. Chin. Inst. Eng.* **2013**, *37*, 807–814. [CrossRef]
6. Liu, S. Study on Construction Control of Negative Bending Moment Area of Steel-concrete Composite Continuous Beam Bridge. *Urban Roads Bridges Flood Control* **2012**, *4*, 142–144. [CrossRef]
7. Bożejko, W.; Hejducki, Z.; Uchroński, M.; Wodecki, M.; Andreev, V. Computer module for scheduling of transportation of composite beam bridge structures. *MATEC Web Conf.* **2016**, *86*, 5015. [CrossRef]
8. Holý, M.; Čítek, D.; Tej, P.; Vráblík, L. The Experimental Timber–UHPC Composite Bridge. *Sustainability* **2021**, *13*, 4895. [CrossRef]
9. Gunes, O.; Yesilmen, S.; Gunes, B.; Ulm, F.-J. Use of UHPC in Bridge Structures: Material Modeling and Design. *Adv. Mater. Sci. Eng.* **2012**, *2012*, 319285. [CrossRef]
10. Greybeal, B. UHPC making strides. *Public Roads* **2009**, *72*, 17–21.
11. Graybeal, B. UHPC in the U.S. highway infrastructure: Experience and outlook. *Indian Concr. J.* **2014**, *88*, 84–91.
12. New Construction Technology for Construction of Huaihe Special Bridge Project in Anhui Section of Jiqi Expressway. *Road Traffic Technol.* **2016**, *12*, 8. Available online: http://www.cnki.com.cn/Article/CJFDTotal-GLJJ201603001.htm (accessed on 1 December 2021).
13. Shi, X.; Ma, H.; Liu, C. Parametric Study and Optimization on Behaviour of Twin-I girder Composite Bridges. *Tongji Daxue Xuebao/J. Tongji Univ.* **2018**, *46*, 444–451.
14. Yaobei, H.; Bofu, F.; Rong, L.; Wenwu, L.; Tingting, L. Mechanical and Economic Study of Small to Medium Span Integral Precast Π-Shaped Steel Plate Combined Beam. *Road Traffic Technol.* **2019**, *36*, 62–68.
15. Gao, Q.; Wu, B.; Li, J.; Cui, K.; Xu, C. Investigation of Traffic Loading Effects for Different Codes on Medium- and Small-Span Girder Bridges in China. *Adv. Civ. Eng.* **2020**, *2020*, 8851981. [CrossRef]
16. Jiang, L.; Feng, Y.; Zhou, W.; He, B. Analysis on natural vibration characteristics of steel-concrete composite truss beam. *Steel Compos. Struct.* **2018**, *26*, 79–87.

17. Chen, A.; Xing, J.; Yang, Q. Numerical Simulation of Construction Process for Large-span Continuous Steel-concrete Composite Bridge. *Sci. Technol. Eng.* **2008**, *8*, 1296–1301.
18. Avci, O.; Bhargava, A. Finite-Element Analysis of Cantilever Slab Deflections with ANSYS SOLID65 3D Rein-forced-Concrete Element with Cracking and Crushing Capabilities. *Pract. Period. Struct. Des. Constr.* **2019**, *24*, 05018007. [CrossRef]
19. Liu, Y.C.; Liu, D.; Wang, Q.P.; Chen, W.D.; Jiang, B. Finite-element Analysis of Composite Energy-Saving Wall Structure with ANSYS. In Proceedings of the Second International Conference on Modelling and Simulation (ICMS2009), Manchester, UK, 21–22 May 2009; Jiang, Y., Ed.; Volume 7, pp. 330–334.
20. Qassim, H.J.; Ali, A. Dynamic response of horizontally curved composite steel I-girder bridges. *Mater. Today Proc.* **2021**, *42*, 1973–1979. [CrossRef]
21. Hou, Z.; Xia, H.; Zhang, Y. Analysis on Natural Vibration Characteristics of a Railway Steel-Concrete Composite Beam Bridge. In Proceedings of the International Conference on Railway Engineering: High-Speed Railway, Heavy Haul Railway and Urban Rail Transit, Beijing, China, 20–21 August 2010.
22. Gunes, B.; Ilki, A.; Oztorun, N.K. Determination of Monitoring Parameters for Fatigue Behaviour of Steel-Concrete Composite Bridge Girders with Welded Full Depth Transverse Stiffeners. *Sustainability* **2020**, *12*, 283. [CrossRef]
23. Gattesco, N. Analytical modelling of nonlinear behaviour of composite beams with deformable connection. *J. Constr. Steel Res.* **1999**, *52*, 195–218. [CrossRef]
24. An, L.; Cederwall, K. Slip and Separation at Interface of Composite Slabs. 1994. Available online: https://scholarsmine.mst.edu/isccss/12iccfss/12iccfss-session6/4/ (accessed on 1 December 2021).
25. Ollgaard, J.G. Shear strength of stud connectors in lightweight and normal weight concrete. *AISC Eng'g Jr.* **1971**, *10*, 55–64.
26. Nie, J.; Cai, C.S. Steel–Concrete Composite Beams Considering Shear Slip Effects. *J. Struct. Eng.* **2003**, *129*, 495–506. [CrossRef]
27. Lee, P.G.; Shim, C.S.; Chang, S.P. Static and fatigue behaviour of large stud shear connectors for steel-concrete composite bridges. *J. Constr. Steel Res.* **2005**, *61*, 1270–1285. [CrossRef]
28. Thomas, J.; Ramaswamy, A. Finite element analysis of shear critical prestressed SFRC beams. *Comput. Concr.* **2006**, *3*, 65–77. [CrossRef]
29. Oehlers, D.; Foley, L. The Fatigue Strength of Stud Shear Connections in Composite Beams. *Proc. Inst. Civ. Eng. Part Res. Theory* **2015**, *79*, 349–364. [CrossRef]
30. Shipo, Z. Study of Mechanical Behaviour of Steel-Concrete Composite Girder Bridge Considering Slip Effect. Ph.D. Thesis, South China University of Technology, Guangzhou, China, 2012.
31. Gao, Q.; Wu, B.; Wang, R.; Zhang, J.; Guo, B.; Li, J. Investigation of the Dynamic Performance of a Large-Span Suspension Bridge Influenced by Scouring Based on Vehicle-Bridge Coupled Vibration. *Shock. Vib.* **2020**, *2020*, 1–12. [CrossRef]
32. Choi, Y.; Lee, J.; Kong, J. Performance Degradation Model for Concrete Deck of Bridge Using Pseudo-LSTM. *Sustainability* **2020**, *12*, 3848. [CrossRef]
33. Sheng, K.J.; Wang, Z.L. Evaluation for Dynamic Performance of Simple-Continuous Bridge. *Adv. Mater. Res.* **2011**, *250-253*, 1360–1365. [CrossRef]
34. Quan, C.; Li, Q.; Deng, J. Load Test and Effect Analysis for Continuous Steel Bridge. *Eng. Test* **2012**, *52*, 23–27.
35. Hwang, E.; Nowak, A.S. Simulation of Dynamic Load for Bridges. *J. Struct. Eng.* **1991**, *117*, 1413–1434. [CrossRef]
36. General Specifications for Design of Highway Bridges and Culverts. In JTG D60-2015, Beijing. 2015; p. 72. Available online: https://xxgk.mot.gov.cn/2020/jigou/glj/202006/t20200623_3312312.html (accessed on 1 December 2021).
37. Qingfei, G. Design and Evaluation Methods for Dynamic Performance of Girder Bridges under Mobile Vehicle Loads. Doctor Type, Harbin Institute of Technology. 2015. Available online: https://d.wanfangdata.com.cn/thesis/D751734 (accessed on 1 December 2021).
38. Hou, Z.; Xia, H.; Wang, Y.; Zhang, Y.; Zhang, T. Dynamic analysis and model test on steel-concrete composite beams under moving loads. *Steel Compos. Struct.* **2015**, *18*, 565–582. [CrossRef]
39. Hastak, M.; Mirmiran, A.; Miller, R.; Shah, R.; Castrodale, R. State of Practice for Positive Moment Connections in Prestressed Concrete Girders Made Continuous. *J. Bridge Eng.* **2003**, *8*, 267–272. [CrossRef]
40. Gao, Q.; Zhang, K.; Wang, T.; Peng, W.; Liu, C. Numerical investigation of the dynamic responses of steel-concrete girder bridges subjected to moving vehicular loads. *Meas. Control.* **2020**, *54*, 465–484. [CrossRef]